# Stratospheric ozone intrusion events and their impacts on tropospheric ozone

Jesse Greenslade[1], Simon Alexander[2], Robyn Schofield[3,4], Jenny A. Fisher[1,5], and Andrew Klekociuk[2]

[1]*Centre for Atmospheric Chemistry, School of Chemistry, University of Wollongong*
[2]*Australian Antarctic Division, Hobart*
[3]*School of Earth Sciences, University of Melbourne*
[4]*ARC Centre of Excellence for Climate System Science, University of New South Wales*
[5]*School of Earth & Environmental Sciences, University of Wollongong*

November 15, 2016

**Abstract**

We develop a quantitative method to identify Stratosphere to Troposphere Transport events (STTs) from ozonesonde profiles. Using this method we estimate the seasonality and quantity of ozone transported across the tropopause over Melbourne (38°S), Macquarie Island (54°S), and Davis (69°S). STT seasonality is determined by two distinct methods using 7–9 years of ozone profiles from each site. The primary method we focus on here shows STT events frequently occurring during summer above all three sites. The majority of tropospheric ozone peaks from by STT events occur within 3 km below the tropopause at Melbourne and Macquarie Island, and within 2 km below the tropopause at Davis. Overall, the fraction of total tropospheric ozone attributed to STT events is 2 4% at each site, however, during individual events, an STT event can contribute more than 10% of the total tropospheric ozone at that time. The meteorological cause of STT events is postulated through visual inspection of ERA-I weather data, with the majority of events caused by low pressure frontal systems at all three sites. Ozone enhancements caused by transported biomass burning plumes are flagged after analysis of CO column measurements from the AIRS satellite. We use the GEOS-Chem model to understand our point-source ozonesonde results in a 3-dimensional context. The GEOS-Chem model is run with active stratospheric chemistry, and is too coarsely resolved in the vertical dimension to determine STTs. Simulated seasonal cycles of tropospheric ozone are well matched at all

three sites although vertical profile averages have some bias in the troposphere compared with ozonesondes. A conservative estimate of yearly tropospheric ozone flux due to STTs are calculated using the simulated tropospheric ozone column between 35°S and 75°S of $3.2 \times 10^{16}$ molecules $cm^{-2}$ $yr^{-1}$. Using an assumed STT impact (of 30%) over the southern ocean rather than our conservative calculation increases the flux estimate to ∼30.2 Tg $yr^{-1}$.

# 1 Introduction

Tropospheric ozone constitutes only 10% of the total ozone column but is an important oxidant and greenhouse gas and is toxic to life, harming natural ecosystems and reducing agricultural productivity. Over the industrial period, increasing tropospheric ozone has been estimated to exert a radiative forcing equivalent to a quarter of the $CO_2$ forcing [Forster et al., 2007]. Further tropospheric ozone enhancements above preindustrial levels are projected to drive reductions in global crop yields equivalent to losses of up to $\$USD_{2000}$ 35 billion per year (simulated until 2030) [Avnery et al., 2013] along with detrimental health outcomes equivalent to ∼11.8 billion per year by 2050 [Selin et al., 2009]. Tropospheric ozone is produced photochemically $NO_x$ and volatile organic compound emissions, which have both anthropogenic (fossil fuel, biomass combustion) and natural (wildfires, lightning, biogenic) sources. In the upper troposphere, downward transport from the ozone-rich stratosphere provides an additional natural source of tropospheric ozone(Jacobson and Hansson [2000] and references therein).

Stratosphere-to-troposphere transport (STT) primarily impacts the ozone budget in the upper troposphere but can also increase regional surface ozone levels above the legal thresholds set by air quality standards [Danielsen, 1968, Lefohn et al., 2011, Langford et al., 2012, Zhang et al., 2014]. A review of two photochemical models by Stohl et al. [2003] concluded that between 25-50% of tropospheric ozone column can be attributed to SST events, although this mostly affects the upper troposphere. A lower estimate was derived from the Atmospheric Chemistry and Climate Model Inter-comparison Project (ACCMIP), Stevenson et al. [2006] found STT was responsible for only ∼ 10% (equivalent to $550 \pm 170$ Tg $yr^{-1}$), with the remainder produced photochemically. The wide range in model estimates exists in part because models are challenged to correctly represent STT. Observation-based process studies are therefore key in determining the relative frequency of SST to the troposphere, with models then able to use this to quantify STT impact over large regions.

STT events are due to deep overshooting convection [Frey et al., 2015], tropical cyclones [Das et al., 2016] and mid-latitude synoptic scale disturbances (e.g. Stohl et al. [2003], Mihalikova et al. [2012]). STT events are strongly dependent on both season and location, for instance over the Mediterranean region, a 10% contribution to tropospheric ozone is estimated between 2000 and 2003 [Galani, 2003], with Lefohn et al. [2011] noting strong seasonal dependence.

Notably, STT events have been shown to contribute up to 30% of the surface ozone over the Western US in spring [Lin et al., 2012].

To date, while the frequency, seasonality, and impacts of STT events have been well characterised in the tropics and Northern Hemisphere (NH), observational estimates from the Southern Hemisphere (SH) extra-tropics are noticeably absent from the literature. Since 1998 NASA has tried to standardise ozonesonde release procedures and improve measurement frequency in the SH through the Southern Hemisphere ADditional OZonesonde (SHADOZ) website (`http://croc.gsfc.nasa.gov/shadoz/`). The papers which have focused on tropospheric ozone in the SH also note the difficulties that arise from sparse datasets, as many of the ozonesonde releases only occur every two to four weeks and far fewer release sites exist compared to the NH [Liu et al., 2015, Thompson et al., 2014, Mze et al., 2010]. This is further complicated due to ozone intrusion events sometimes lasting for just a matter of hours [Tang and Prather, 2012]. Recently ozonesondes were analysed showing upper tropospheric ozone is increasing near southern Africa, with the increase most likely due to stratospheric mixing [Liu et al., 2015, Thompson et al., 2014]. The extra-tropics in the SH have even fewer observational studies published.

In the extra-tropics, ozone has a longer photochemical lifetime(TODO: how long?) and STT events most commonly occur during synoptic-scale tropopause folds [Sprenger et al., 2003, Tang and Prather, 2012], and are characterised by tongues of high potential vorticity (PV) air descending to low altitudes. As these tongues become elongated, filaments disperse away from the tongue and mix irreversibly into the troposphere. To date, STT events have been observed in tropopause folds around both the polar front jet [Vaughan et al., 1993, Beekmann et al., 1997], and the subtropical jet [Baray et al., 2000]. They are also observed near cut-off lows [Price and Vaughan, 1993, Wirth, 1995], some of the stratospheric mixing may be due to the turbulent weather which often accompanies these cut-offs. A high correlation has been found between lower stratospheric and tropospheric ozone concentrations [Terao et al., 2008], suggesting mixing between these two layers, with jet streams over the ocean being the major source of transport between the layers.

Ozonesondes are useful for looking at specific locations with high resolution, and in this work they provide an estimate of both STT occurrence rates and STT ozone flux. At these discrete locations, this information can be used in conjunction with regional-scale information in order to estimate large-scale impacts of STT on tropospheric ozone. Here, the GEOS-Chem chemical transport model (CTM) is used to provide the regional-scale ozone concentrations.

Here, we use nearly a decade of ozonesonde observations from three locations spanning latitudes from 38°S - 69°S to characterise the seasonal cycle of STT events and quantify their contribution to the tropospheric ozone budget. In Section 2 we describe the observations and the methods used to identify STT. In Section 3 we examine two case studies to relate STT occurrence to meteorological events. Section 4 provides our newly derived climatologies of STT frequency, seasonality, intrusion altitude, and depth. Section 5 uses these new climatologies to evaluate tropospheric ozone in a global chemical transport

model (GEOS-Chem). Finally, we use the observations and the model to estimate the overall contribution of STT events to total tropospheric ozone in the high southern latitudes.

# 2 Data and Methods

## 2.1 Ozonesonde record in the Southern Ocean

Ozonesondes provide a high vertical resolution profile of ozone, temperature, pressure, and humidity from the surface to 35 km.

Ozone mixing ratio is quantified with an electrochemical concentration cell that senses the proportional electrical current from reaction of ozone with a solution of potassium iodide. Standardised procedures are followed when constructing, transporting, and releasing the ozonesondes [NOAA]. Ozonesondes are estimated to provide around 2% precision in the stratosphere, which improves at lower altitudes [NOAA], and ozonesondes have been shown to be accurate to within 5% as long as the correct procedures are followed [Smit et al., 2007].

Ozonesondes are launched approximately weekly from Melbourne (38°S, 145°E), Macquarie Island (55°S, 159°E) and Davis (69°S, 78°E). For this study, we use the data collected from 2004-2013 for Melbourne and Macquarie, and 2006-2013 for Davis. This is because at these dates we have both ozone and geopotential height (GPH) profiles from the ozonesondes at these sites. At Davis, ozonesondes are launched twice as frequently in the months just prior to and during the ozone hole season (June-October) as at other times of the year [Alexander et al., 2013].

Stratospheric ozone typically mixes irreversibly (vertically and horizontally) into the troposphere in kilometre-scale tongues of air [Frey et al., 2015]. The strength (ozone enhancement above background levels), horizontal scale, vertical depth, and longevity of these intruding ozone tongues vary with weather, topography, and season. This makes the vertical ozone profile recorded by the ozonesonde highly dependent on the time of launch [Sprenger et al., 2003], and it cannot be guaranteed that detected ozone enhancements are fully separated from the stratosphere.

Characterisation of STT events requires a clear definition of the tropopause. The two most common tropopause height definitions are the standard lapse rate tropopause [WMO, 1957] and the ozone tropopause [Bethan et al., 1996]. The lapse rate tropopause is defined as the lowest altitude where the lapse rate (gradient of temperature with altitude) is less than 2° C $km^{-1}$, provided the lapse rate between this altitude and all subsequent altitudes within 2 km is also below 2° C $km^{-1}$. The ozone tropopause is defined as the lowest altitude satisfying the following three conditions for the ozone mixing ratio (OMR) [Bethan et al., 1996]:

1. Vertical gradient of OMR is greater than 60 ppb $km^{-1}$

2. OMR is greater than 80 ppb

3. OMR exceeds 110 ppb between 500 m and 2000 m above the altitude under inspection (500 m and 1500 m in the Antarctic, including the site at Davis).

The ozone tropopause can be less robust during stratosphere-troposphere exchange, however it is more robust than the lapse rate tropopause at polar latitudes in winter and near jet streams in the lower stratosphere due to temperature inversions near the tropopause definition region [Bethan et al., 1996, Tomikawa et al., 2009, Alexander et al., 2013]. In this work the lower of these two tropopause altitudes is used, as both are calculated for each ozonesonde release. Here, we calculate both tropopause heights for each ozonesonde release and use whichever is lower. This choice avoids occasional unrealistically high tropopause heights due to perturbed ozone or temperature measurements in the ozonesonde data.

Figure 1 shows the monthly mean tropopause altitudes at each location (solid lines). The dashed lines in Figure 1 show the mean tropopause altitude calculated from the subset of ozonesondes that detected an STT event. The seasonal cycle in tropopause altitude at Melbourne is exhibited, showing a maximum in summer, and a minimum is winter. This cycle is much more subtle at Macquarie, and almost reversed at Davis, which has a minimum during autumn and maximum from winter to spring. The decreasing tropopause altitude which occurs at higher southern latitudes is also apparent, as lower mean tropopause heights occur with more southern latitudes. The tropopause is higher on days with an STT event at all during winter and sprint at Davis.

Figure 2 shows multi-year averaged ozone mixing ratios measured by ozonesonde over the three stations. Over Melbourne, increased ozone extending down through the troposphere is apparent from December to March and September to November. The increased tropospheric ozone in these months are due to STTs (in summer), and possible fire smoke plume influence (in winter), discussed in more detail below. Over Davis and Macquarie Island, the tropospheric ozone is higher between March and October, although the seasonal differences are small compared to those at Melbourne. This seasonality at the high latitude sites is driven by a decrease in photochemical destruction when the solar zenith angle is greater, causing light to have longer path length and reduced radiation (TODO: read and cite S. Oltmans antarctic papers - re Andrews comment).

## 2.2 Model description

GEOS-Chem is a global chemical transport model [Bey et al., 2001], which includes transport, emission, deposition, chemical production and destruction of ozone and 103 other trace gases throughout the troposphere along with stratospheric chemistry, including photolysis. Stratosphere-troposphere coupling is calculated using the stratospheric unified chemistry extension (UCX) [Eastham et al., 2014], which includes a further 28 trace gases. For comparison to ozonesonde observations, we use GEOS-Chem version 10-011 (including UCX)

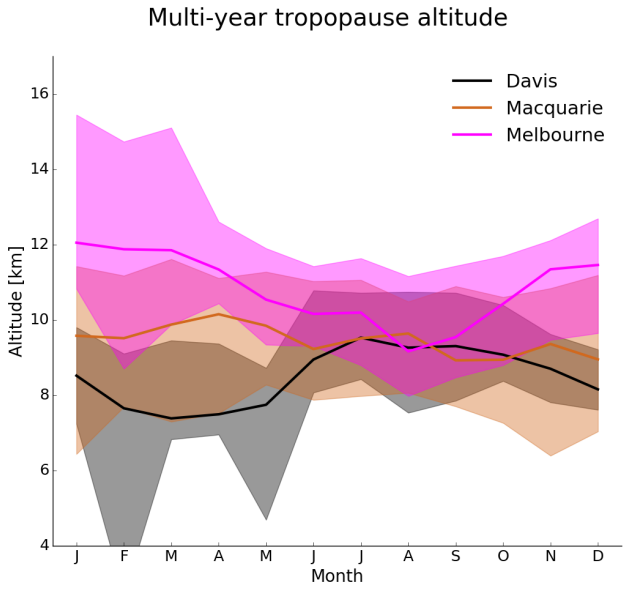


Figure 1: Multi-year monthly median tropopause altitude (minimum of lapse rate and ozone defined tropopause) determined from ozonesondes measurements at Melbourne (2004-2013), Macquarie (2004-2013) and Davis (2006-2013) (solid lines). Vertical shading shows the 10th to the 90th percentile of tropopauses for each site.

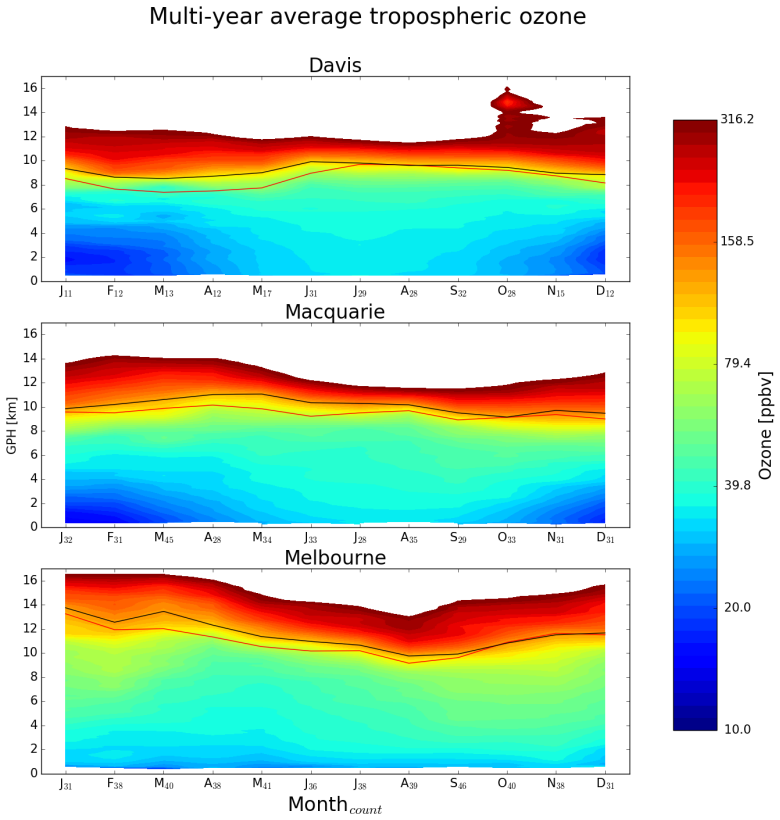


Figure 2: Multi-year mean seasonal cycle of ozone mixing ratio over Davis, Macquarie, and Melbourne measured by ozonesondes. Measurements were interpolated to every 100 m and then binned monthly. Black, red solid lines show median ozone and lapse-rate tropopause altitudes, defined as described in the text.

run from 2005-2012, following a 1-year spin-up for 2004. Transport is driven by assimilated meteorological fields from the Goddard Earth Observing System (GEOS-5) maintained by the Global Modeling and Assimilation Office (GMAO) at NASA. Biogenic emissions of organic chemicals are determined by the Model of Emissions of Gases and Aerosols from Nature (MEGAN) version 2.1 extended by Guenther et al [Guenther et al., 2012]. Anthropogenic emissions are given by the Emissions Database for Global Atmospheric Research (EDGAR) version 4.2.

Our simulation was modified from the standard v10-01 to a fix a bug in the treatment of the Total Ozone Mapping Spectrometer (TOMS) satellite data used to calculate photolysis (see Henderson [2016]). The simulation uses 2° latitude by 2.5° longitude horizontal resolution, with 72 vertical levels from the surface to 0.1 hPa. The profile stored at each site is the average within the grid boxes which contain the site. For each site, a vertical profile of ozone is stored every 6 hours, based on standard UTC+0 time. This means that the GEOS-Chem profiles which match ozonesonde release hours are local times of 7AM, 11AM, and 11AM for Davis, Macquarie, and Melbourne respectively.

## 2.3 Characterisation of STT events and associated fluxes

We characterise STT events using the ozonesonde vertical profiles to identify tropospheric ozone volume mixing ratio enhancements above a local background (in moles per billion moles of dry air, or ppb). Calculation of ozone transport is performed after converting the profile to molecules $cm^{-3}$. The process is illustrated in Figure 3 for an example ozone profile.

First, the ozone vertical profiles are linearly interpolated to a regular grid with 20 m resolution from the surface to 14 km altitude. The interpolated profiles are then bandpass filtered using a Fourier transform to retain perturbations with vertical scales between 0.5 km and 5 km (removing low and high frequency perturbations). In what follows, these filtered vertical profiles are referred to as perturbation profiles. The choice of band limits was set empirically. For an event to qualify as STT, a clear increase above the background ozone level is needed, and we find that a vertical limit of $\sim$ 5 km removes seasonal-scale effects. The 0.5 km scale limit is set in order to remove any spikes of ozone which could be considered noise. We next use all the perturbation profiles at each site to calculate the 99th percentile perturbation value for the site. This is considered our threshold for tropospheric ozone perturbations, and perturbations above this threshold in individual ozonesondes are classified as STT events.

STTs which occur at altitudes below 4 km are removed in order to avoid surface pollution events Those occurring within 0.5 km of the tropopause are also removed in order to avoid spurious false positives induced by the sharp transition to stratospheric air.

Finally, we define the ozone peak as the altitude where the OMR is greatest within the lowest range of altitudes where the perturbation profile exceeds the percentile-based threshold. If the perturbation profile drops below zero between the ozone peak and the tropopause, the STT event is confirmed. Alternatively,

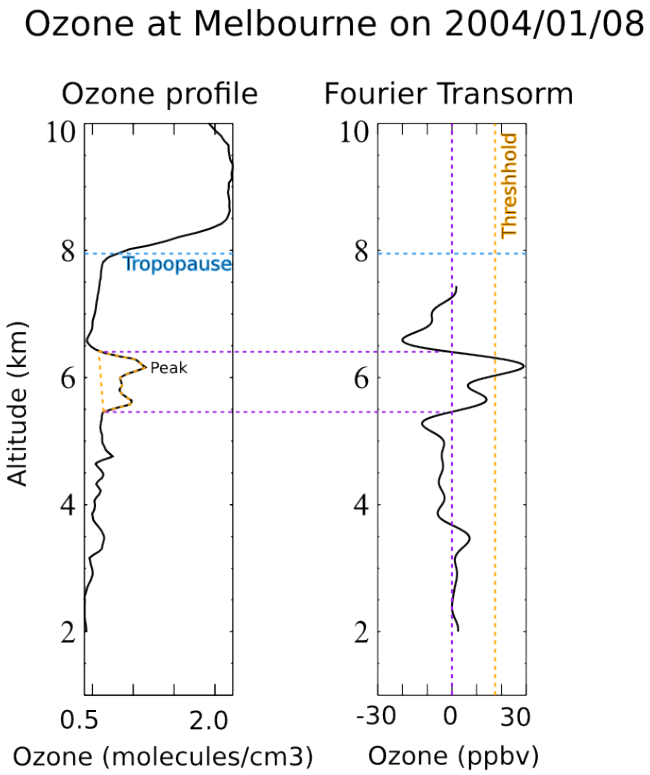


Figure 3: An example of the STT identification and flux estimation methods used in this work. The left panel shows an ozone mixing ratio profile from Melbourne on the 8th of January 2004 from 2km to the tropopause (dashed horizontal line). The right panel shows the perturbation profile created from bandpass filtering of the mixing ratio profile. The STT occurrence threshold calculated from the 99th percentile of filtered ozone perturbations is shown with the orange dashed line, and the technique for determining the vertical extent of the event is shown with the purple dashed lines (see details in text). The ozone flux associated with the STT event is calculated using the area outlined with the orange dashed line in the left panel.

if the OMR between the ozone peak and the tropopause drops below 80 ppb and is at least 20 ppb lower than the OMR at the ozone peak, the STT event is also confirmed. Otherwise the profile is rejected as a non-event. This final step removes near-tropopause anomalies for which there is no evidence of detachment from the stratosphere.

We estimate the ozone flux into the troposphere associated with each event by integrating the ozone concentration enhancement vertically over the altitude range for which an STT event is identified (i.e. the range surrounding the ozone peak over which the perturbation profile is greater than zero). This estimate is conservative because it does not take into any secondary ozone enhancements that may have been caused by the STT, and also ignores any heightened ozone background levels which may be due to synoptic-scale stratospheric mixing into the troposphere.

Tang and Prather [2010] define one possible method for detecting STT events from ozonesonde measurements. Their definition is based on subjective analysis of sondes released from 20 stations in the latitudinal range from 35°S to 40°N. In their work, a tropopause fold has occurred if, starting from 5 km altitude, the ozone level exceeds 80 ppb and then within 3 km decreases by 20 ppb or more to a value less than 120 ppb.

## 2.4 Biomass burning influenced events

The STT detection algorithm described in Section 2.3 assumes all mid-upper troposphere ozone perturbations above the 99th percentile are caused by stratospheric intrusions. In some cases, however, these perturbations may in fact reflect ozone production in lofted smoke plumes. Biomass burning in southern Africa and South America has previously been shown to have a major influence on atmospheric composition in the vicinity of our measurement sites [Oltmans et al., 2001, Gloudemans et al., 2007, Edwards et al., 2006], particularly from July to December [Pak et al., 2003]. The downwind effects of biomass burning smoke plumes from South America and southern Africa are strongest around August and September, as seen here and in Liu et al. [2016]. On occasion, smoke plumes from Australian and Indonesian fires can also reach the mid-high southern latitudes, which is seen when examining the carbon monoxide (CO) from the AIRS (Atmospheric Infrared Sounder) instrument on board the Aqua satellite [AIR, 2013].

Large biomass burning events emit substantial quantities of ozone precursors, some of which are capable of being transported long distances and driving ozone production far from the fire source [Jaffe and Wigder, 2012]. Ozone production from biomass burning is complex and affected by photochemistry, fuel nitrogen load, and time since emission. While ozone production occurs in some biomass burning plumes, this is not always the case; therefore ozone perturbations detected during transported smoke events may or may not be caused by the plume. We therefore flag all detected STT events found near smoke plumes but do not exclude them from our final dataset.

Possible biomass burning influence is identified using satellite observations

of CO from the AIRS instrument. CO is emitted during incomplete combustion and is an effective tracer of long-range transport due to its long lifetime. In the Southern Hemisphere, biomass burning is the primary source of CO, making CO a good proxy for fire plumes (eg: Edwards [2003], Sinha et al. [2004], Edwards et al. [2006], Mari et al. [2008]).(TODO: split citations to their most appropriate sentences) We use data from the AIRS (Atmospheric Infrared Sounder) instrument on board the Aqua satellite [AIR, 2013]. To identify possible biomass burning influence, we visually inspected AIRS vertical columns CO in the vicinity of our three measurement sites for all dates with detected STT events. We diagnose smoke plumes as areas with elevated CO columns ($\sim 2 \times 10^{18}$ molecules cm$^{-2}$ or higher), and flag any sonde-detected STT event that occurs near a smoke plume.

Figure 4 contrasts two days with and without signs of biomass burning influence near the Melbourne site (purple circle). 17 October 2007 (top) shows a day where elevated CO suggests the site may have been influenced by long-range transport from African and/or South American biomass burning. In contrast, on 3 February 2006 (bottom) CO columns across the Southern Hemisphere show no influence from biomass burning. We screened all days with detected STT events except one event during which there were no available AIRS data (January 2010), and found that biomass burning may have influenced 21% of events over Melbourne and 17% of events over Macquarie island. These events are flagged in the following sections, and are not used in our calculation of total STT flux. All of the flagged events except for one (in January at Macquarie Island) occur within the Southern Hemisphere burning season (July to December).No events at Davis were influenced by smoke transport.

## 2.5 Sensitivities and limitations

Our method uses several subjectively defined quantities in the process of STT event detection. Here we briefly discuss these and the sensitivity to each. Using the algorithm discussed in section 2.3, we detect 45 events at Davis, 47 (+8 fire influenced) events at Macquarie Island, and 72(+14 fire influenced) events at Melbourne.

The cut-off threshold (defined separately for each site) is determined from the 99th percentile of the ozone perturbations between 2 km and 1 km below the tropopause. We use the 99th percentile because at this point the filter locates clear events with no obvious false positives. Event detection is highly sensitive to this choice; for example, using the 98.5th percentile instead increased detected events by 24 at Melbourne (33%), 19 at Macquarie Island (40%), and 10 at Davis (22%). This high sensitivity means that detection is also sensitive to the profile altitude bounds used in calculation of the percentiles, i.e. the 2 km altitude to 1 km below the tropopause range. The altitude range used to determine the 99th percentile is set from 2 km up to 1 km below the tropopause. This range removes any anomalous edge effects of the Fourier bandpass filter, as well as discounting the highly variable ozone concentration which occurs near the tropopause. Finally, ozone enhancements are only considered STT events

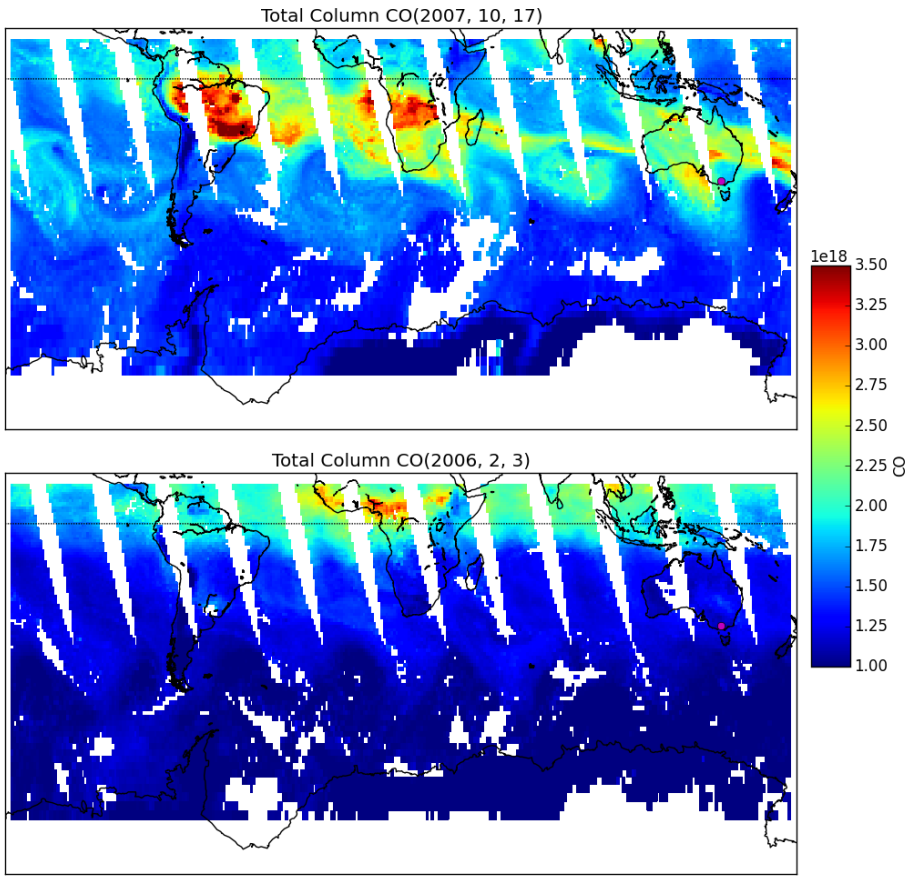


Figure 4: Example detection of biomass burning influence using AIRS total column CO. The top panel (17 October 2007) shows a day when ozone above Melbourne (purple dot) could have been caused by a transported biomass burning plume, and so was flagged in subsequent analysis. The bottom panel (3 February 2006) shows a day when Melbourne ozone was not influenced by transported smoke.

if they occur above 4 km and within 500 m below the tropopause. This range removes possible ground pollution, as well as allowing event detection up to 500 m from the tropopause. Some events, including the storm-caused event examined in figure 5 are within one kilometer of the tropopause.

The event detection was not as sensitive to the choice of Fourier bandpass scales; A widening of the allowed scales to the range 0.4-5.1 increased the detected events by 3 at Melbourne, 2 at Macquarie Island, and Davis lost two events (there are more detected events, but more being filtered out).

Flux estimation over the southern ocean is based on the average GEOS-Chem tropospheric vertical column of HCHO over a particular latitude range. The range is from 35°S to 75°S, changing this latitude range by 5° in either direction at either end of the range changes the average simulated tropospheric ozone by -8 to 9%.

## 2.6 Classifying synoptic conditions during STT events

An investigation of the ERA-I synoptic weather during STT events above (at 500 hPa) Melbourne, Macquarie Island, and Davis are used to subjectively classify the events based on their likely cause. Typically during STT occurrence, the upper troposphere is not calm, with low pressure fronts or cut-offs nearby at coincident time. Similar characteristics are seen over Melbourne and Macquarie Island: i.e. a prevalence of frontal and low pressure activity during STT events. Over Davis the weather systems are harder to distinguish, and the stratospheric polar vortex may create ozone folds without other sources of upper tropospheric turbulence.

We examine two case studies in detail to illustrate the synoptic-scale conditions in which STT events occur over Melbourne. Data from the European Center for Medium-range Weather Forecasts (ECMWF) Interim Reanalysis (ERA-I) [Dee et al., 2011] product are used for synoptic-scale examination of weather patterns over our three sites on dates matching detected STT events.

Figure 5 (left) shows the ozonesonde profile above Melbourne on 3 of February 2005. The tropopause was between 400 and 500 hPa and ozone in the upper troposphere was anticorrelated with relative humidity, suggesting the ozone enhancements derived from dry stratospheric air. An ozone intrusion into the troposphere at $\sim$ 520 hPa was identified by our detection algorithm. Figure 5(right) shows the concurrent synoptic weather system, a cut-off low pressure system that caused a large storm and lowered the local tropopause height for several days. These systems also increase turbulence near the tropopause, which can lead to increased transport events. The flux of stratospheric ozone into the troposphere associated with this event, calculated using the method shown in section 2.3, was at least $3.1 \times 10^{11}$ molecules cm$^{-3}$ , or 8% of the tropospheric ozone column.

Figure 6 (left) shows the ozonesonde profile over Melbourne on 13 January 2010. The tropopause was higher on this date (120-160 hPa). Using our algorithm, we detected an ozone intrusion centred around 200 hPa. As before, ozone anti-correlation with relative humidity provides further evidence that

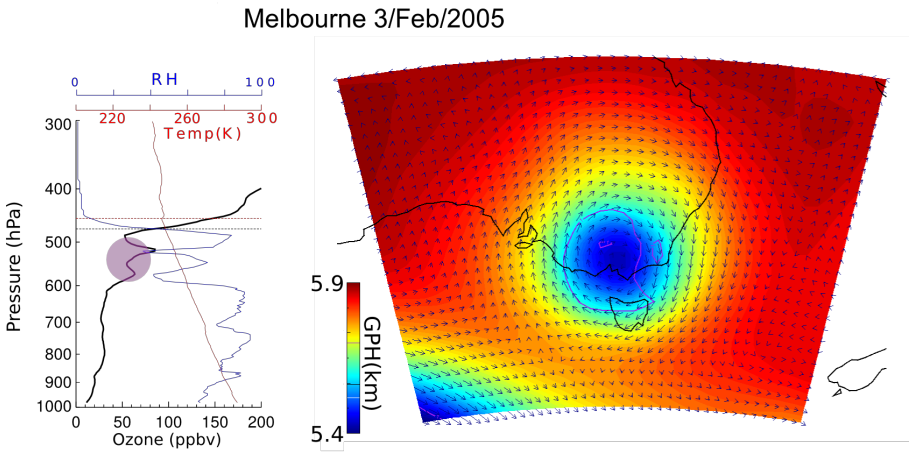


Figure 5: (Left) Vertical profile of ozone (black), relative humidity (blue), and temperature (red) measured by ozonesonde over Melbourne on 3 February 2005. The detected ozone STT event is highlighted in pink. Tropopause heights using both the ozone definition (black dashed line) and lapse rate definition (red dashed line) are also shown. (Right) Geopotential heights at 500 hPa from the ERA-Interim reanalysis, with wind vectors overplotted. Also shown are contours of potential vorticity units with 1 PVU in purple.

the elevated ozone was stratospheric in origin. In this profile, there was clear separation between the detected intrusion (highlighted in pink) and the ozone tropopause (black dashed line), which indicates that the sonde passed through regular tropospheric air after hitting a stratospheric intrusion but before reaching the tropopause. Figure 6 (right) shows that this event was associated with a trough of low pressure (front) passing over southeastern Australia. This front traveled from west to east and caused a wave of lowered tropopause height. Frontal passage is a known cause of STT as stratospheric air descends and streamers of ozone-rich air break off and mix into the troposphere [Sprenger et al., 2003].

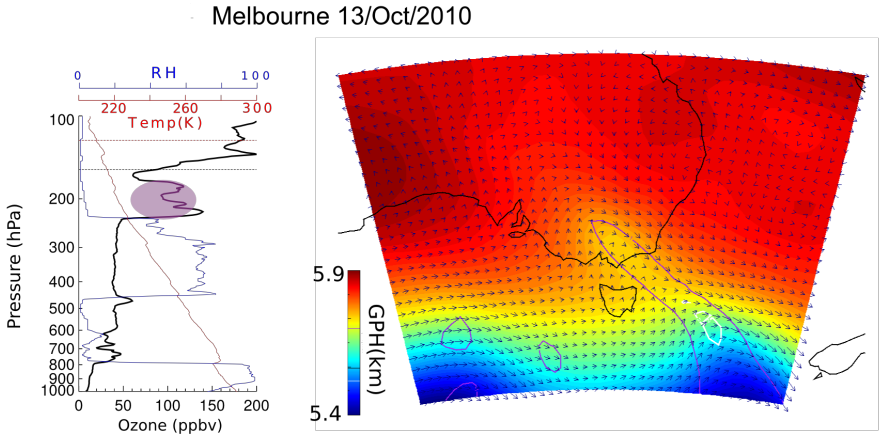


Figure 6: Same as Figure 5 but for 13 January 2010. Also shown in this figure is the 2 PVU contour (white), often used to determine dynamical tropopause height.

# 3 STT event climatologies

Figure 7 shows the seasonal cycles of STT events detected at Melbourne, Macquarie Island, and Davis. STT events in Figures 7-10 are coloured based on the meteorological classification described in Section 2.6, with events classified as either low pressure fronts (frontal, dark blue), cut-off low pressure systems (cutoff, teal), or indeterminate (misc, cyan). Events that may have been influenced by transported smoke plumes (Section 2.4) are shown in red. Ozonesonde releases and detected event counts are summarised in table 1.

There is an annual cycle in the frequency of STT events (Fig. 7) with a summertime peak above All three sites. This summertime peak is due to an increased prevalence of summer low-pressure storms and fronts, which increase

| Site | Sondes | Events | Cut-offs | Frontals | Fire |
|---|---|---|---|---|---|
| Davis | 240 | 45 | 7 | 20 | 0 |
| Macquarie | 390 | 47 | 10 | 25 | 8 |
| Melbourne | 456 | 72 | 15 | 40 | 14 |

Table 1: Summary of ozonesonde releases, detected events, and category of the events. Categories are described in the text.

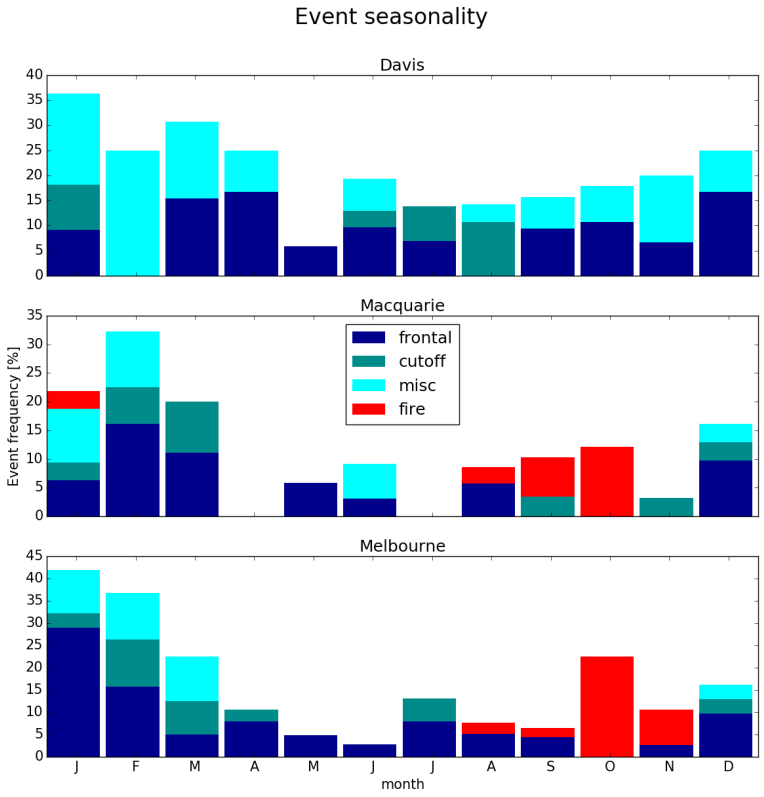


Figure 7: Seasonal cycle of STT events detected at Davis (top), Macquarie Island (middle), and Melbourne (bottom). Events are categorised by associated meteorological conditions as described in the text, with low pressure fronts (frontal) in dark blue, cut-off low pressure systems (cutoff) in teal, and indeterminate meteorology (misc) in cyan. Events that may have been influenced by transported smoke plumes are shown in red (see text for details).

turbulence and lower the tropopause [Reutter et al., 2015]. For both Melbourne and Macquarie Island, the STT events which are unlikely to be fire-related occur mostly in summer during these low pressure synoptic systems.

At Davis, the frequency of STT events is relatively constant throughout the year, with a slight increase during Antarctic summer. STT events associated with cut-off low pressure systems are more prevalent during summer (spring for Davis), while STT events associated with frontal passage occur throughout the year. The polar vortex and associated lowered tropopause may be partially responsible for the STTs detected in winter.

To examine the robustness of the distributions shown in Fig 7, we developed an alternative assessment of the seasonal occurrence of STT events and the results from this assessment are shown in Figure 8. Here STT occurrence is evaluated by consideration of the square of the dry Brunt-Visl frequency ($N^2$) at the heights of the ozone tropopause ($z_{OT}$) lapse rate tropopause ($z_{LRT}$) in each ozonesonde profile that has been binned to 500 m resolution. We use N2 to assess atmospheric stability, which is normally distinctly higher in the stratosphere than in the troposphere, and assume that the vertical temperature gradients within the intrusion respond most rapidly to transported heat, which is an additional characteristic of stratospheric air. The altitude binning chosen is a compromise between vertical resolution and the level of variability in $N^2$ introduced by temperature gradients associated with perturbations from gravity waves and changes near the lapse rate tropopause, and is the minimum that produces a robust seasonal distribution. We define STT as having taken place if $N^2(z_{OT}) > N^2(z_{LRT})$ and $z_{OT} < z_{LRT}$; in this way the characteristically higher static stability and ozone concentration of stratospheric intrusion is regarded as being retained as it penetrates below the lapse rate tropopause. The seasonal distributions shown for the three stations in Fig. 8 are generally similar to those shown in Fig. 7, with the main exception that no events are identified with the alternative method at Davis in the first half of the year. For the months December to June, ozonesondes are generally only launched monthly at Davis, and the lack of STT events in these months for Davis shown in Fig. 8 potentially reflects the fewer measurement opportunities.

Figure 9 shows the altitudes of detected events, based on the altitude of peak (maximum) tropospheric ozone in the ozonesonde profile. STT event peaks most commonly occur at 6 – 10 km above Melbourne and 6 – 9 km at Davis but are distributed more evenly at Macquarie Island from 4 – 7.5 kilometres altitude. There is no clear relationship between meteorological conditions and event altitude.

Figure 10 shows the distance from the tropopause of the peaks of detected events, based on the distance between the peak ozone peak associated with the detected STT event and the tropopause (using the lowest of the two tropopause definitions), as described in Section 2.1. The majority of STT events occur within 3 km of the tropopause at both Melbourne and Macquarie Island, and within 2 km of the tropopause at Davis. Again, there is no clear relationships between meteorological conditions and event depth.

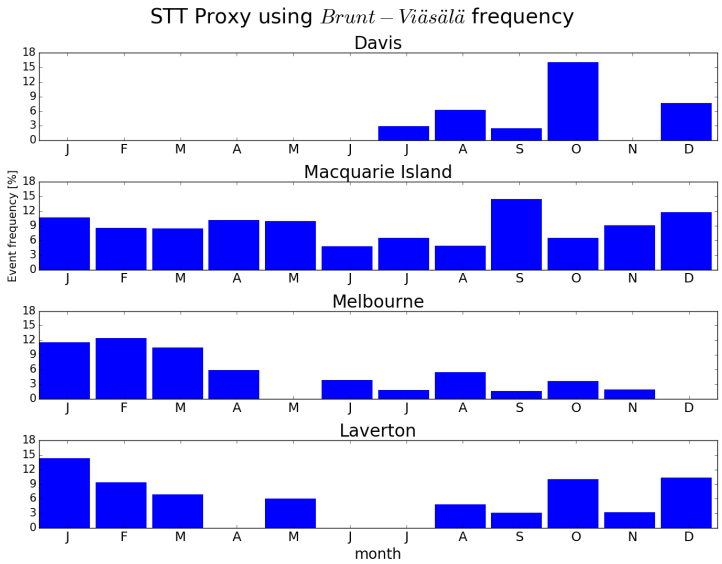


Figure 8: Seasonal distribution of the STT proxy, obtained from consideration of the static stability at the ozone and lapse rate tropopauses, for Melbourne (1999-2012), Macquarie Island (1994-2012) and Davis (2003-2012). Data for Laverton is also included (1984-1999).

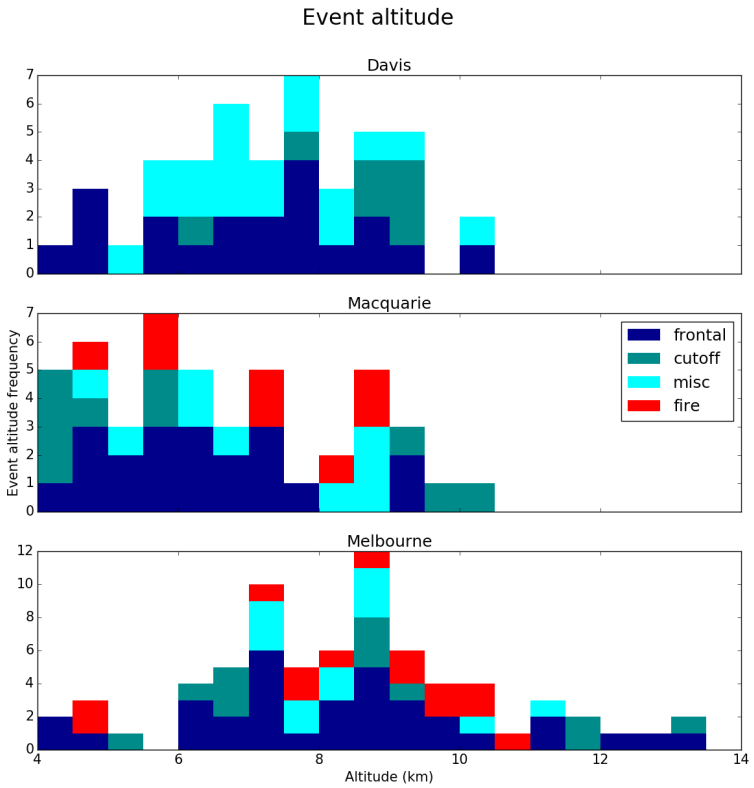


Figure 9: The distribution of STT event altitude at Davis (top), Macquarie Island (middle), and Melbourne (bottom), determined as described in the text. Events are coloured as described in Fig. 7.

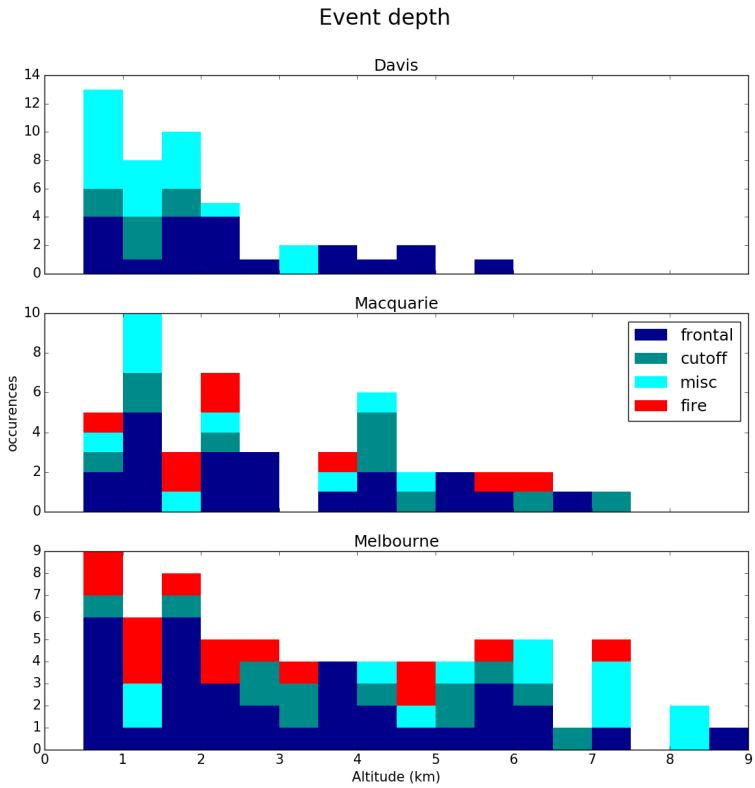


Figure 10: The distribution of STT event distance from the tropopause at Davis (top), Macquarie Island (middle), and Melbourne (bottom), determined as described in the text. Events are coloured as described in Fig. 7.

# 4 Comparison with GEOS-Chem

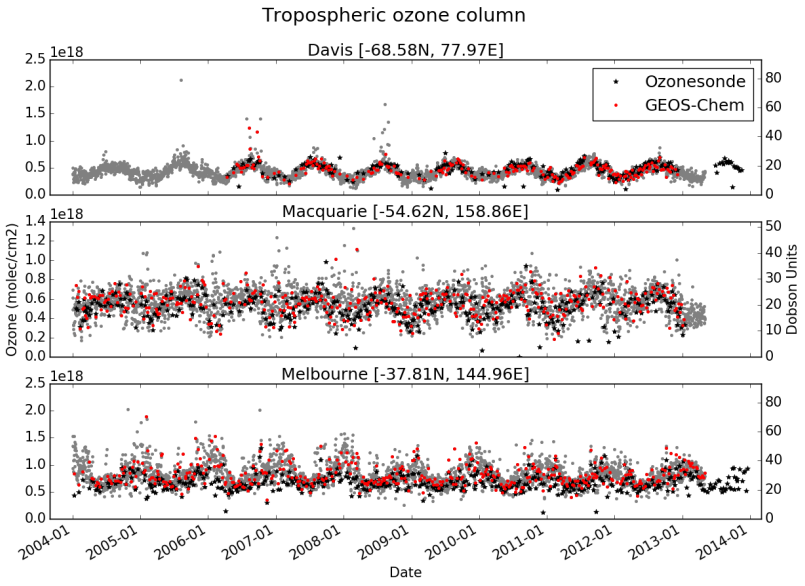


Figure 11: Tropospheric ozone column ($\Omega_{O3}$, in molecules cm$^{-2}$) at daily resolution simulated by GEOS-Chem (grey dots) from January 1 2004 to April 31 2013. Simulated points which are on the same day as an ozonesonde are displayed in red. For each plot, the model has been sampled in the grid square containing the site. Columns calculated from ozonesondes are shown as black stars, each representing one measurement.

Figure 11 compares the time series of tropospheric ozone column ($\Omega_{O_3}$) in molecules cm$^{-2}$ simulated by GEOS-Chem (red dots) to the measured tropospheric ozone columns (black stars). Sonde tropospheric columns are calculated using ozone partial pressure ($P_{HCHO}$) and temperature (T) recorded by the ozonesondes to determine the molec cm$^{-3}$, using the ideal gas law and integrating with the recorded GPH up to the tropopause:

$$\frac{n_{HCHO}}{V} = \frac{P_{HCHO}}{RT}\Omega_{HCHO} = \int_0^{\mathrm{TP}} \frac{n_{HCHO}}{V} \times N_{Av}\mathrm{d}z$$

The seasonal cycles of $\Omega_{HCHO}$ from ozonesondes appear to have similar season and magnitude as the modeled $\Omega_{HCHO}$. In both observations and model, the maximum ozone column at Melbourne occurs in summer, with a minimum in winter, while Macquarie and Davis show the opposite seasonality.

Using reduced major axis regression to calculate the line of best fit gives a near one to one slope for all sites, with the most divergent site (Melbourne)

having a slope of 1.33. The paired $r^2$ values for Davis, Macquarie, Melbourne respectively are 0.38, 0.18, 0.37 between the observed and modelled tropospheric columns. Removing the seasonality by subtracting the multi-year mean monthly values from GEOS-Chem and ozonesonde data lowers the $r^2$ values to .07, .12, .30 respectively, however the slope of all the regressions remains near (within 10% of) 1.

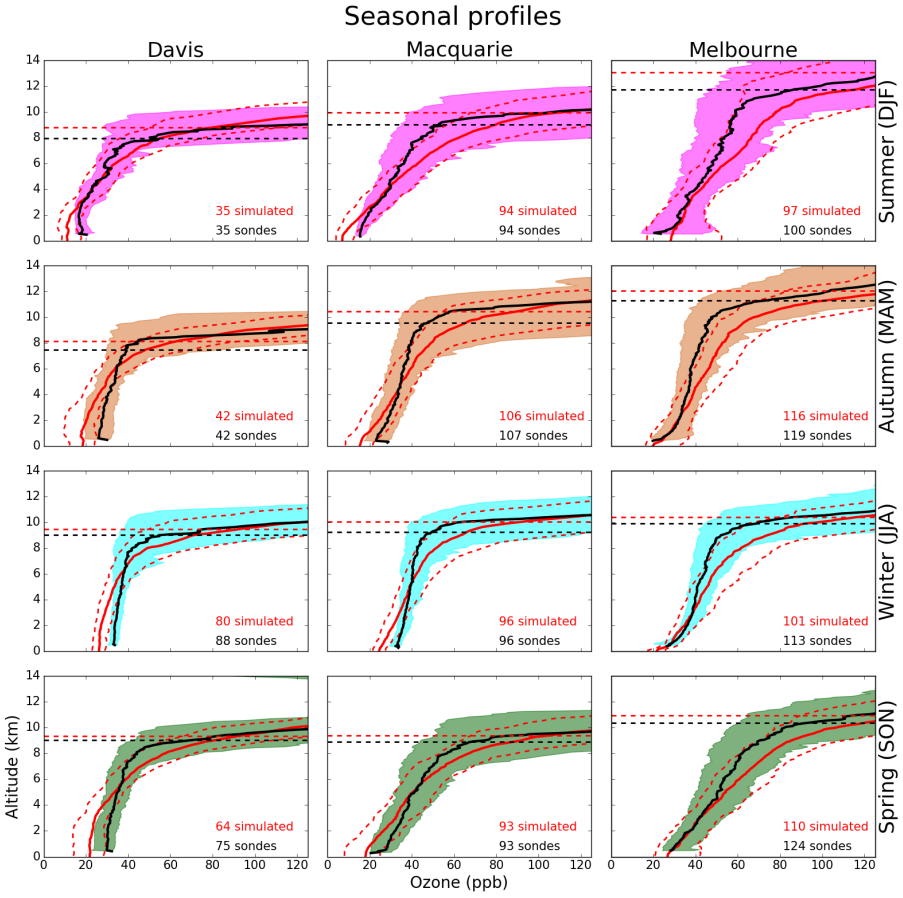


Figure 12: Observed and simulated tropospheric ozone profiles over Davis, Macquarie, and Melbourne, averaged seasonally. Model means (2005-2013 average) is shown as red solid lines, with red dashed lines showing the 10th and 90th percentile. Ozonesonde means (over each season, for all years) are shown as black solid lines, with coloured shaded areas showing the 10th and 90th percentile. The horizontal dotted line shows the mean tropopause heights from the model (red) and the observations (black).

Figure 12 shows the observed and simulated ozone profiles at all sites, aver-

aged seasonally. The model generally underestimates ozone at low altitudes (up to 6 km) at both Davis and Macquarie, although this bias is less pronounced during summer. Over Melbourne, ozone in the lower troposphere is well represented, but the model overestimates ozone from around 4 km to the tropopause. Also shown is the tropopause height simulated by the model (horizontal dashed red line), the mean of which is always higher than the observed average, although this difference is statistically insignificant. The effect of local pollution can be seen over Melbourne, mostly during the austral summer months (DJF), as the increased mean mixing ratios and enhanced variance near the surface.

Although GEOS-Chem reasonably matches the ozonesonde tropospheric ozone column, it does not have the resolution required to capture STT events. Figure 13 compares modeled (red) and observed (black) ozone profiles on three example days when STT events were detected using the ozonesondes. The plot shows the profile with the closest (qualitative) match between model and observations; from left to right the profiles are from Davis (Sep. 2006), Macquarie Island (Dec. 2012), and Melbourne (Feb. 2010). The vertical resolution from GEOS-Chem is too low to allow detection of STTs, with roughly 30 vertical levels up to the tropopause, while ozonesondes have upwards of 100, although in a few cases (eg. Melbourne in figure 13) it appears that the event was large enough to be clearly visible in the GEOS-Chem output.

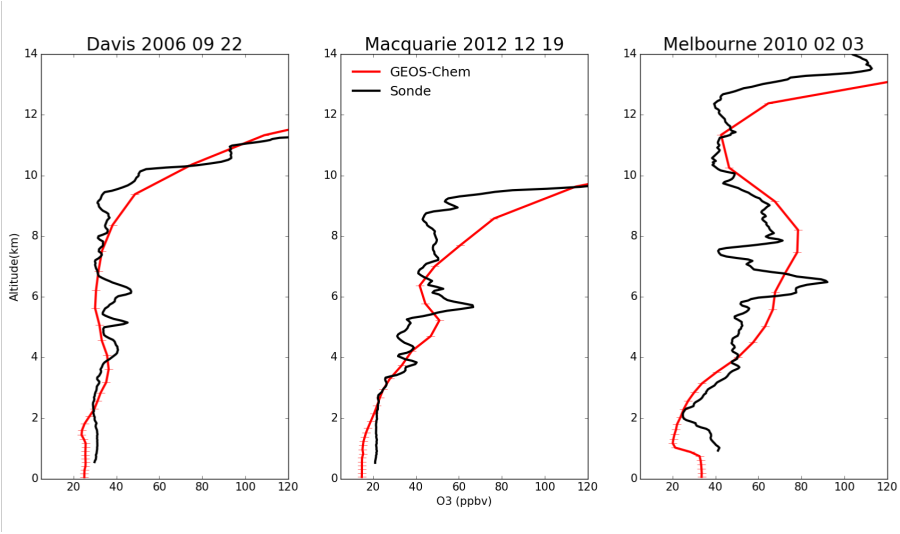


Figure 13: Example comparisons of ozone profiles from ozonesondes (black) and GEOS-Chem (red) from three different dates during which STT events were detected from the measurements. The dates were picked based on subjective visual analysis. The examples show the best match between model and observations for each site. GEOS-Chem pressure levels are marked with a dash.

# 5 Stratosphere-to-troposphere ozone flux from STT events

We quantify the mean stratosphere-to-troposphere ozone flux due to STT events at each site based on the integrated ozone amount associated with each STT event (see section 2.3). Events that may have been influenced by transported biomass burning are excluded from this calculation. This estimate is a conservative lower bound as our algorithm ignores secondary ozone peaks which may also be transported down from the stratosphere and also potential ozone enhancement due to the ozone intrusion which is outside the event positive perturbation range around the detected ozone peak.

Figure 15 shows the mean fraction of total tropospheric column ozone calculated from ozonesonde profiles at each site attributed to stratospheric ozone intrusions, averaged over days when an STT event occurred. At all sites, the mean fraction of tropospheric ozone attributed to STT events is 2–4%. On individual days, this value can exceed 10% at Macquarie and Melbourne. Figure 14 shows the STT-induced ozone flux in absolute terms. We find that the mean ozone flux associated with STT events is 1 to 2 $\times 10^{16}$ molecules cm$^{-2}$. Our flux estimates are relatively insensitive to our biomass burning filter: including smoke-influenced days changed the mean flux by less than 5% relative to the absolute absolute values.

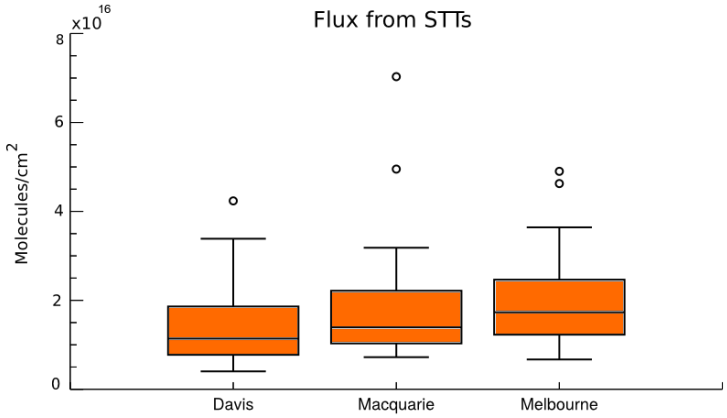


Figure 14: Tropospheric ozone attributed to STT, derived from ozonesonde measurements as described in the text. Box shows the interquartile range (IQR), with the centre line being the median, whiskers show the minimum and maximum, circles show values which lie more than 1.5 IQR from the median.

We use simulated tropospheric ozone columns from GEOS-Chem to extrapolate the ozonesonde-based estimates to the entire Southern Ocean region. To do so, we multiply the monthly likelihoods of STTs (fraction of ozonesonde re-

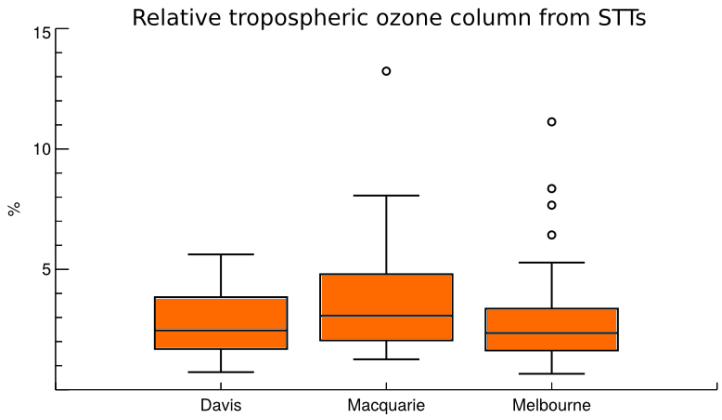


Figure 15: Fraction of total tropospheric column ozone attributed to STT, derived from ozonesonde measurements as described in the text.

leases for which an STT event was detected, per month, 'l') by the monthly mean tropospheric ozone column over the Southern Ocean (from the GEOS-Chem multi-year mean, $\Omega_{SO_{O_3}}$) and by the monthly mean fraction of the ozone column attributed to STT ('f') (as in Fig. 15, but separated by month). The monthly values of each term in this equation are shown in Figure 16 (lower panel). The equation can be written simply: Flux= $\Omega_{SO_{O_3}} \times f \times l$.

Figure 16 shows the extrapolated monthly mean ozone flux from STT events over the Southern Ocean. We find that STT events may be responsible for at least $3.2 \times 10^{16}$ molecules cm$^{-2}$ yr$^{-1}$, of the tropospheric ozone over the Southern Ocean, this is around 2.57 Tg yr$^{-1}$ ozone. This is calculated using the surface area from GEOS-Chem over the southern ocean grid boxes along with the molecules cm$^{-2}$ per month calculations, along with ozone molar mass of 48 g mol$^{-1}$.

Our estimate is far less than other estimates of STT flux, due to our conservative estimate of flux within each event, as well as filtering out events which are too close to the tropopause. Global STT flux estimated from an ensemble of models suggests values around 550 Tg yr$^{-1}$ [Stevenson et al., 2006]. Global net downward STT flux is estimated to be 75 Tg yr$^{-1}$ [Sprenger et al., 2003]. Our estimate of 2.57 Tg yr$^{-1}$ is $\sim$3.42% of this value, which is quite a bit lower. This method of flux estimation could be increased if we could account for background ozone enhancement and mixing due to events. This highlights one of the difficulties with temporally sparse ozonesonde data. Our flux calculation only looks at a particular type of ozone event and may be unsuitable for comparison with total or net STT flux.

Olsen [2003] use PV and winds from the GEOS reanalysis combined with ozone measurements from the TOMS satellite to estimate that around 210 Tg

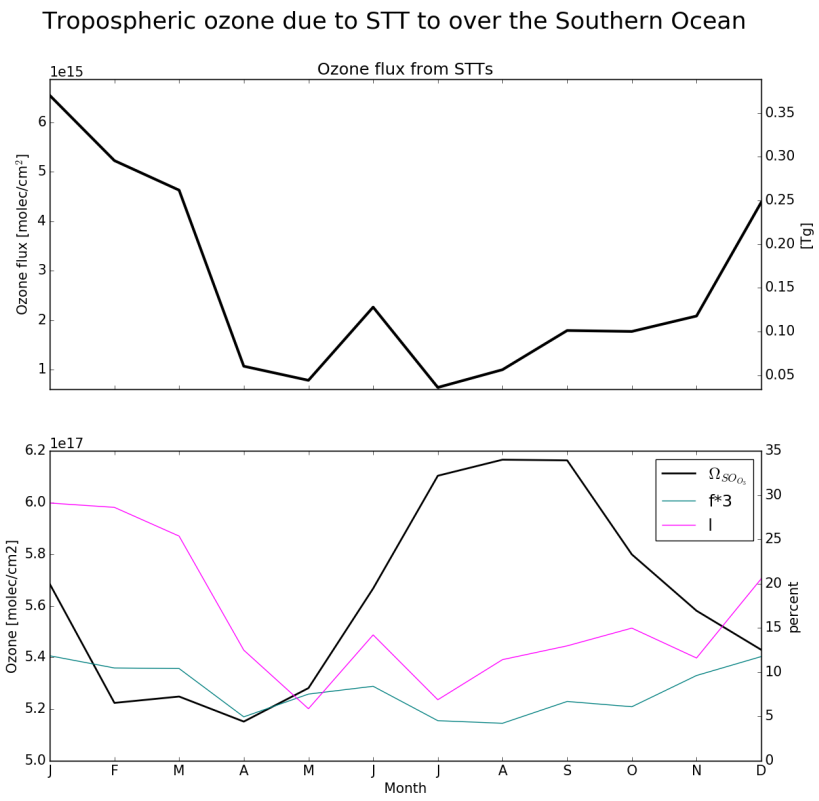


Figure 16: (Top) Estimated contribution of STT to tropospheric ozone columns over the Southern Ocean. (Bottom) The three quantities used to calculate (as per the text) the flux estimates shown in the top panel. The tropospheric ozone column (left axis) is from GEOS-Chem, while the STT fraction and likelihoods (right axis) are from the ozonesonde measurements. The STT fraction is multiplied by 3 to show the seasonality.

$yr^{-1}$ of ozone flux occurs in 2000 between 30°S and 60°S. Their estimates show peak ozone flux from winter to early spring (JJAS). Liu et al. [2016] model the upper tropospheric ozone and it's source (emissions/lightning/stratospheric) over the Atlantic ocean between 30°S and 45°S, and suggest that most of this is transported from the stratosphere from March to September, which is when the subtropical jet system is strongest. At this time of year, we find from the GEOS-Chem simulation the highest overall tropospheric $\Omega_{O3}$, but a relatively low overall STT flux. Our results suggest that the STT flux (due to tropopause fold style events) is largest in austral summer (DJFM), primarily due to an increased frequency of STT detections during these months. Some legitimate STT events may have been removed due to coincident smoke plumes, which could affect our STT event frequency during winter. It is worth noting that the 30°S to 60°S latitudes describe the Ferrel cell, while our region of analysis also includes some of the Polar cell.

Considering the individual event contributions, Terao et al. [2008] estimate much higher STT impacts using a global CTM with a stratospheric ozone tracer; where 30–40% of the 500 hPa ozone is due to STT. Although this figure is based on the Northern Hemisphere upper troposphere, if we assume that STT flux due to an event is actually 35% (instead of using our estimated influence) our estimate increases by roughly a factor of 12: to ∼30.2 Tg $yr^{-1}$ This would suggest that tropopause fold ozone transport events over the southern ocean account ∼40.3% of global net STT flux.

# 6 Conclusions

Ozonesonde data in the Southern Hemisphere provides a satellite-independent quantification of STT ozone transport. The frequency and amount of ozone descending from the stratosphere into the troposphere can be estimated from the long time series of tropospheric ozone profiles. Using almost ten years of ozonesonde profiles over the southern high latitudes, a clear summer peak is seen for STT occurrences at our three sites (38°S, 55°S, and 69°S).

We use a Fourier bandpass filter to determine STT ozone transport events. The filter removes seasonal tropospheric ozone influences and allows clear detection of ozone-enhanced tongues of air in the troposphere. By setting empirical checks, ozonesonde vertical profiles can clearly show tropospheric ozone enhancement which is separated from the stratosphere. This method is sensitive to some parameters, but can determines clear tropospheric ozone peaks from our record of ozonesondes.

The cause of these ozone enhancements is examined through the use of satellite CO data (to determine fire influence) and ERA-I meteorological data. The major causes of STT events found over each of our sites are turbulent weather in the upper troposphere due to low pressure fronts, with the next most likely cause being either cut-off low pressure systems or undetermined. All three sites show a summer (DJF) maximum and winter (JJA) minimum, although the seasonal amplitude is less apparent at Davis, as winter and spring events are

regularly detected.

Integration of the ozone enhancement along the altitude of the ozone profile allows a rough estimate of stratospheric transport for each event. Our conservative ozone flux calculation typically estimates that 3% of the tropospheric ozone column is due to a particular STT event. Within a year this ranges from 1 to $6 \times 10^{15}$ molecules $cm^{-2}$ ozone enhancement over the southern high latitudes caused by STT. Further work needs to be done to quantify STT flux using solely ozonesonde data, more frequent ozonesonde releases would make this easier.

GEOS-Chem estimates of the tropospheric ozone column match fairly well with the ozonesonde observations, with least squares regression correlation coefficient ($r^2$) of 0.38, 0.18, 0.37, for Davis, Macquarie, and Melbourne respectively. Using reduced major axis regression (which does not assume that there is no error in the measurements) there is a near one to one slope at all three sites, with or without removing the seasonality of both GEOS-Chem and the ozonesondes. Our STT detection algorithm is unsuitable for GEOS-Chem output, as the model averages over 2° latitude by 2.5° longitude grid boxes, with a lower vertical resolution (especially in the upper troposphere). Due to their high vertical resolution ozonesondes are able to detect STT events where reanalysis datasets or models may not.

# References


AIRS3STD, 2013.

S. P. Alexander, D. J. Murphy, and A. R. Klekociuk. High resolution VHF radar measurements of tropopause structure and variability at Davis, Antarctica (69?? S, 78?? E). *Atmospheric Chemistry and Physics*, 13(6):3121–3132, 2013. ISSN 16807324. doi: 10.5194/acp-13-3121-2013. URL `http://www.atmos-chem-phys.net/13/3121/2013/`.

Shiri Avnery, Denise L. Mauzerall, Junfeng Liu, and Larry W. Horowitz. Global crop yield reductions due to surface ozone exposure: 2. Year 2030 potential crop production losses and economic damage under two scenarios of O 3 pollution. *Atmospheric Environment*, 71(13):408–409, 2013. ISSN 13522310. doi: 10.1016/j.atmosenv.2012.12.045. URL `http://dx.doi.org/10.1016/j.atmosenv.2011.01.002`.

J. L. Baray, V. Daniel, G. Ancellet, and B. Legras. Planetary-scale tropopause folds in the southern subtropics. *Geophysical Research Letters*, 27(3):353–356, 2000. ISSN 00948276. doi: 10.1029/1999GL010788.

M. Beekmann, G. Ancellet, S. Blonsky, D. De Muer, A. Ebel, H. Elbern, J. Hendricks, J. Kowol, C. Mancier, R. Sladkovic, H. G J Smit, P. Speth, T. Trickl, and Ph Van Haver. Regional and global tropopause fold occurrence and related ozone flux across the tropopause. *Journal of Atmospheric Chemistry*, 28(1-3):29–44, 1997. ISSN 01677764. doi: 10.1023/A:1005897314623.

S. Bethan, G. Vaughan, and S. J. Reid. A comparison of ozone and thermal tropopause heights and the impact of tropopause definition on quantifying the ozone content of the troposphere. *Quarterly Journal of the Royal Meteorological Society*, 122(532):929–944, 1996. ISSN 00359009. doi: 10.1002/qj.49712253207. URL http://doi.wiley.com/10.1002/qj.49712253207.

Isabelle Bey, Daniel J. Jacob, Robert M. Yantosca, Jennifer A. Logan, Brendan D. Field, Arlene M. Fiore, Qin-Bin Li, Hong-Yu Liu, Loretta J. Mickley, and Martin G. Schultz. Global Modeling of Tropospheric Chemistry with Assimilated Meteorology: Model Description and Evaluation. *Journal of Geophysical Research*, 106:73–95, 2001. ISSN 0148-0227. doi: 10.1029/2001JD000807.

Edwin F. Danielsen. Stratospheric-Tropospheric Exchange Based on Radioactivity, Ozone and Potential Vorticity, 1968. ISSN 0022-4928.

S S Das, M V Ratnam, K N Uma, K V Subrahmanyam, and I A Girach. Influence of tropical cyclones on tropospheric ozone : possible implication. *Atmospheric Chemistry and Physics (Discussions)*, 15(2003):19305–19323, 2016. ISSN 1680-7324. doi: 10.5194/acpd-15-19305-2015.

D P Dee, S M Uppala, A J Simmons, P Berrisford, P Poli, S Kobayashi, U Andrae, M A Balmaseda, G Balsamo, P Bauer, P Bechtold, A C M Beljaars, L van de Berg, J Bidlot, N Bormann, C Delsol, R Dragani, M Fuentes, A J Geer, L Haimberger, S B Healy, H Hersbach, E V HÃlm, L Isaksen, P KÃllberg, M KÃ¶hler, M Matricardi, A P McNally, B M Monge-Sanz, J.-J. Morcrette, B.-K. Park, C Peubey, P de Rosnay, C Tavolato, J.-N. ThÃ©paut, and F Vitart. The ERA-Interim reanalysis: configuration and performance of the data assimilation system. *Quarterly Journal of the Royal Meteorological Society*, 137(656):553–597, 2011. ISSN 1477-870X. doi: 10.1002/qj.828. URL http://dx.doi.org/10.1002/qj.828.

Sebastian D. Eastham, Debra K. Weisenstein, and Steven R H Barrett. Development and evaluation of the unified tropospheric-stratospheric chemistry extension (UCX) for the global chemistry-transport model GEOS-Chem. *Atmospheric Environment*, 89:52–63, 2014. ISSN 13522310. doi: 10.1016/j.atmosenv.2014.02.001. URL http://dx.doi.org/10.1016/j.atmosenv.2014.02.001.

D. P. Edwards. Tropospheric ozone over the tropical Atlantic: A satellite perspective. *Journal of Geophysical Research*, 108(D8):4237, 2003. ISSN 0148-0227. doi: 10.1029/2002JD002927. URL http://doi.wiley.com/10.1029/2002JD002927.

D. P. Edwards, L. K. Emmons, J. C. Gille, A. Chu, J. L. Attié, L. Giglio, S. W. Wood, Jim Haywood, M. N. Deeter, S. T. Massie, D. C. Ziskin, and James R. Drummond. Satellite-observed pollution from Southern Hemisphere biomass burning. *Journal of Geophysical Research Atmospheres*, 111(14):1–17, 2006. ISSN 01480227. doi: 10.1029/2005JD006655.

P. Forster, V. Ramaswamy, P. Artaxo, T. Berntsen, R. Betts, D.W. Fahey, J. Haywood, J. Lean, D.C. Lowe, G. Myhre, J. Nganga, R. Prinn, G. Raga, M. Schulz, and R. Van Dorland. Changes in Atmospheric Constituents and in Radiative Forcing. In: Climate Change 2007: The Physical Science Basis. Contribution of Working Group I to the Fourth Assessment Report of the Intergovernmental Panel on Climate Change[Solomon, S., D. Qin, M. Man, 2007. URL https://www.ipcc.ch/publications_and_data/ar4/wg1/en/ch2.html.

W. Frey, R. Schofield, P. Hoor, D. Kunkel, F. Ravegnani, a. Ulanovsky, S. Viciani, F. D'Amato, and T. P. Lane. The impact of overshooting deep convection on local transport and mixing in the tropical upper troposphere/lower stratosphere (UTLS). *Atmospheric Chemistry and Physics*, 15 (11):6467–6486, 2015. ISSN 1680-7324. doi: 10.5194/acp-15-6467-2015. URL http://www.atmos-chem-phys.net/15/6467/2015/.

E. Galani. Observations of stratosphere-to-troposphere transport events over the eastern Mediterranean using a ground-based lidar system. *Journal of Geophysical Research*, 108(D12):1–10, 2003. ISSN 0148-0227. doi: 10.1029/2002JD002596. URL http://www.agu.org/pubs/crossref/2003/2002JD002596.shtml.

Annemieke Gloudemans, Jos De Laat, Maarten Krol, Jan Fokke Meirink, Guido Van Der Werf, Hans Schrijver, and Ilse Aben. Evidence for long-range transport of carbon monoxide in the Southern Hemisphere from SCIAMACHY observations. *European Space Agency, (Special Publication) ESA SP*, 33 (SP-636):1–5, 2007. ISSN 03796566. doi: 10.1029/2006GL026804.

A. B. Guenther, X. Jiang, C. L. Heald, T. Sakulyanontvittaya, T. Duhl, L. K. Emmons, and X. Wang. The model of emissions of gases and aerosols from nature version 2.1 (MEGAN2.1): An extended and updated framework for modeling biogenic emissions. *Geoscientific Model Development*, 5(6):1471–1492, 2012. ISSN 1991959X. doi: 10.5194/gmd-5-1471-2012.

Ben Henderson. TOMS OH Fix, 2016. URL http://wiki.seas.harvard.edu/geos-chem/index.php/FAST-JX_v7.0_photolysis_mechanism#Fix_for_TOMS_to_address_strange_cycle_in_OH_output.

M C Jacobson and H Hansson. Organic atmospheric aerosols: Review and state of the science. *Reviews of Geophysics*, (38):267–294, 2000. ISSN 87551209. doi: 10.1029/1998RG000045.

Daniel a. Jaffe and Nicole L. Wigder. Ozone production from wildfires: A critical review. *Atmospheric Environment*, 51:1–10, 2012. ISSN 13522310. doi: 10.1016/j.atmosenv.2011.11.063. URL http://dx.doi.org/10.1016/j.atmosenv.2011.11.063.

A. O. Langford, J. Brioude, O. R. Cooper, C. J. Senff, R. J. Alvarez, R. M. Hardesty, B. J. Johnson, and S. J. Oltmans. Stratospheric influence on surface ozone in the Los Angeles area during late spring and early summer of 2010. *Journal of Geophysical Research Atmospheres*, 117(3):1–17, 2012. ISSN 01480227. doi: 10.1029/2011JD016766.

Allen S. Lefohn, Heini Wernli, Douglas Shadwick, Sebastian Limbach, Samuel J. Oltmans, and Melvyn Shapiro. The importance of stratospheric-tropospheric transport in affecting surface ozone concentrations in the western and northern tier of the United States. *Atmospheric Environment*, 45(28):4845–4857, 2011. ISSN 13522310. doi: 10.1016/j.atmosenv.2011.06.014. URL `http://dx.doi.org/10.1016/j.atmosenv.2011.06.014`.

Meiyun Lin, Arlene M. Fiore, Owen R. Cooper, Larry W. Horowitz, Andrew O. Langford, Hiram Levy, Bryan J. Johnson, Vaishali Naik, Samuel J. Oltmans, and Christoph J. Senff. Springtime high surface ozone events over the western United States: Quantifying the role of stratospheric intrusions. *Journal of Geophysical Research Atmospheres*, 117(19):1–20, 2012. ISSN 01480227. doi: 10.1029/2012JD018151.

Junhua Liu, Jose M. Rodriguez, Anne M. Thompson, Jennifer A. Logan, Anne R. Douglass, Mark A. Olsen, Stephen D. Steenrod, and Françoise Posny. Origins of tropospheric ozone interannual variation over Réunion: A model investigation. *Journal of Geophysical Research Atmospheres*, pages 1–19, 2015. doi: 10.1002/2015JD023981. URL `http://onlinelibrary.wiley.com/doi/10.1002/2015JD023981/abstract`.

Junhua Liu, Jose M. Rodriguez, Stephen D. Steenrod, Anne R. Douglass, Jennifer A. Logan, Mark Olsen, Krzysztof Wargan, and Jerald Ziemke. Causes of interannual variability of tropospheric ozone over the Southern Ocean. *Atmospheric Chemistry and Physics Discussions*, (October):1–46, 2016. ISSN 1680-7316. doi: 10.5194/ACP-2016-692.

C H Mari, G Cailley, L Corre, M Saunois, Atti E, J L, V Thouret, and A Stohl. Tracing biomass burning plumes from the Southern Hemisphere during the AMMA 2006 wet season experiment, Atmos. *Atmospheric Chemistry and Physics*, 8:3951–3961, 2008. ISSN 1680-7324. doi: 10.5194/acpd-7-17339-2007.

M Mihalikova, S Kirkwood, J Arnault, and D Mikhaylova. Observation of a tropopause fold by MARA VHF wind-profiler radar and ozonesonde at Wasa, Antarctica: comparison with ECMWF analysis and a WRF model simulation. *Annales Geophysicae*, 30(9):1411–1421, 2012. doi: 10.5194/angeo-30-1411-2012. URL `http://www.ann-geophys.net/30/1411/2012/`.

N. Mze, A. Hauchecorne, H. Bencherif, F. Dalaudier, and J. L. Bertaux. Climatology and comparison of ozone from ENVISAT/GOMOS and SHADOZ/balloon-sonde observations in the southern tropics. *Atmospheric*

*Chemistry and Physics*, 10(16):8025–8035, 2010. ISSN 16807316. doi: 10.5194/acp-10-8025-2010.

NOAA. NOAA Ozone sondes appendix. URL `http://www.ndsc.ncep.noaa.gov/organize/protocols/appendix5/`.

Mark a. Olsen. A comparison of Northern and Southern Hemisphere cross-tropopause ozone flux. *Geophysical Research Letters*, 30(7):1412, 2003. ISSN 0094-8276. doi: 10.1029/2002GL016538. URL `http://doi.wiley.com/10.1029/2002GL016538`.

J Oltmans, J Johnson, M Harris, J Bendura, A Logan, and Jioji Tabuadravu. Ozone in the Pacific tropical troposphere from ozonesonde observations. 106, 2001.

B.C.a Pak, R.L.b Langenfelds, S.A.b Young, R.J.b Francey, C.P.b Meyer, L.M.b Kivlighon, L.N.b Cooper, B.Lb Dunse, C.E.b Allison, L.P.b Steele, IE.b Galbally, and I.A.b Weeks. Measurements of biomass burning influences in the troposphere over southeast Australia during the SAFARI 2000 dry season campaign. *Journal of Geophysical Research D: Atmospheres*, 108(13):SAF 16–1 – SAF 16–10, 2003. ISSN 0148-0227. doi: 10.1029/2002JD002343. URL `http://www.scopus.com/inward/record.url?eid=2-s2.0-0742322536&partnerID=40&md5=cafaeef03b948fb456696583ed3ab9a5`.

J. D. Price and G. Vaughan. The potential for stratosphere-troposphere exchange in cut-off-low systems. *Quarterly Journal of the Royal Meteorological Society*, 119(510):343–365, 1993. doi: 10.1002/qj.49711951007. URL `http://onlinelibrary.wiley.com/doi/10.1002/qj.49711951007/abstract`.

P. Reutter, B. Škerlak, M. Sprenger, and H. Wernli. Stratosphere-troposphere exchange (STE) in the vicinity of North Atlantic cyclones. *Atmospheric Chemistry and Physics*, 15(19):10939–10953, 2015. ISSN 16807324. doi: 10.5194/acp-15-10939-2015.

N E Selin, S Wu, K M Nam, J M Reilly, S Paltsev, R G Prinn, and M D Webster. Global health and economic impacts of future ozone pollution. *Environmental Research Letters*, 4(4):044014, 2009. ISSN 1748-9326. doi: 10.1088/1748-9326/4/4/044014.

Parikhit Sinha, Lyatt Jaeglé, Peter V. Hobbs, and Qing Liang. Transport of biomass burning emissions from southern Africa. *Journal of Geophysical Research*, 109:D20204, 2004. ISSN 01480227. doi: 10.1029/2004JD005044.

Herman G J Smit, Wolfgang Straeter, Bryan J. Johnson, Samuel J. Oltmans, Jonathan Davies, David W. Tarasick, Bruno Hoegger, Rene Stubi, Francis J. Schmidlin, T. Northam, Anne M. Thompson, Jacquelyn C. Witte, Ian Boyd, and Françoise Posny. Assessment of the performance of ECC-ozonesondes under quasi-flight conditions in the environmental simulation chamber: Insights

from the Juelich Ozone Sonde Intercomparison Experiment (JOSIE). *Journal of Geophysical Research Atmospheres*, 112(19):1–18, 2007. ISSN 01480227. doi: 10.1029/2006JD007308.

Michael Sprenger, Mischa Croci Maspoli, and Heini Wernli. Tropopause folds and cross-tropopause exchange: A global investigation based upon ECMWF analyses for the time period March 2000 to February 2001. *Journal of Geophysical Research: Atmospheres*, 108(D12):n/a—-n/a, 2003. ISSN 2156-2202. doi: 10.1029/2002JD002587. URL `http://dx.doi.org/10.1029/2002JD002587`.

D S Stevenson, F J Dentener, M G Schultz, K Ellingsen, T P C van Noije, O Wild, G Zeng, M Amann, C S Atherton, N Bell, D J Bergmann, I Bey, T Butler, J Cofala, W J Collins, R G Derwent, R M Doherty, J Drevet, H J Eskes, A M Fiore, M Gauss, D A Hauglustaine, L W Horowitz, I S A Isaksen, M C Krol, J.-F. Lamarque, M G Lawrence, V Montanaro, J.-F. Müller, G Pitari, M J Prather, J A Pyle, S Rast, J M Rodriguez, M G Sanderson, N H Savage, D T Shindell, S E Strahan, K Sudo, and S Szopa. Multimodel ensemble simulations of present-day and near-future tropospheric ozone. *J. Geophys. Res.*, 111(D8), 2006. doi: 10.1029/2005jd006338. URL `http://dx.doi.org/10.1029/2005JD006338`.

Andreas Stohl, Heini Wernli, Paul James, Michel Bourqui, Caroline Forster, Mark A. Liniger, Petra Seibert, and Michael Sprenger. A new perspective of stratosphere-troposphere exchange. *Bulletin of the American Meteorological Society*, 84(11):1565–1573+1473, 2003. ISSN 00030007. doi: 10.1175/BAMS-84-11-1565.

Q. Tang and M. J. Prather. Correlating tropospheric column ozone with tropopause folds: The Aura-OMI satellite data. *Atmospheric Chemistry and Physics*, 10(19):9681–9688, 2010. ISSN 16807316. doi: 10.5194/acp-10-9681-2010.

Q. Tang and M. J. Prather. Five blind men and an elephant: can NASA Aura measurements quantify the stratosphere-troposphere exchange of ozone flux? *Atmospheric Chemistry and Physics*, 11(5):2357–2380, 2012. ISSN 16807316. doi: 10.5194/acp-12-2357-2012. URL `http://dx.doi.org/10.5194/acpd-11-26897-2011`.

Yukio Terao, Jennifer A Logan, Anne R Douglass, and Richard S Stolarski. Contribution of stratospheric ozone to the interannual variability of tropospheric ozone in the northern extratropics. *J. Geophys. Res.*, 113(D18), 2008. doi: 10.1029/2008jd009854. URL `http://dx.doi.org/10.1029/2008jd009854`.

A. M. Thompson, N. V. Balashov, J. C. Witte, J. G R Coetzee, V. Thouret, and F. Posny. Tropospheric ozone increases over the southern Africa region: Bellwether for rapid growth in Southern Hemisphere pollution? *Atmospheric Chemistry and Physics*, 14(18):9855–9869, 2014. ISSN 16807324. doi: 10.5194/acp-14-9855-2014.

Yoshihiro Tomikawa, Yashiro Nishimura, and Takashi Yamanouchi. Characteristics of Tropopause and Tropopause Inversion Layer in the Polar Region. *SOLA*, 5:141–144, 2009. doi: 10.2151/sola.2009-036. URL `http://dx.doi.org/10.2151/sola.2009-036`.

G Vaughan, J D Price, and A Howells. Transport into the troposphere in a tropopause fold. *Quarterly Journal of the Royal Meteorological Society*, 120 (518):1085–1103, 1993. ISSN 00359009. doi: 10.1002/qj.49712051814.

Volkmar Wirth. Diabatic heating in an axisymmetric cut-off cyclone and related stratosphere-troposphere exchange. *Quarterly Journal of the Royal Meteorological Society*, 121(521):127–147, 1995. ISSN 00359009. doi: 10.1002/qj.49712152107. URL `http://doi.wiley.com/10.1002/qj.49712152107`.

World Meteorological Organization WMO. Meteorology A Three-Dimensional Science. *Geneva, Second Session of the Commission for Aerology*, 4:134–138, 1957.

L Zhang, D J Jacob, X Yue, N V Downey, D A Wood, and D Blewitt. Sources contributing to background surface ozone in the US Intermountain West. *Atmos. Chem. Phys.*, 14(11):5295–5309, 2014. doi: 10.5194/acp-14-5295-2014. URL `http://dx.doi.org/10.5194/acp-14-5295-2014`.